SIAM J. Applied Dynamical Systems
Vol. 9, No. 1, pp. 238–260

Localized States in a Model of Pattern Formation in a Vertically Vibrated Layer*

J. H. P. Dawes† and S. Lilley‡

Abstract. We consider a novel asymptotic limit of model equations proposed to describe the formation of localized states in a vertically vibrated layer of granular material or viscoelastic fluid. In physical terms, the asymptotic limit is motivated by experimental observations that localized states ("oscillons") arise when regions of weak excitation are nevertheless able to expel material rapidly enough to reach a balance with diffusion. Mathematically, the limit enables a novel weakly nonlinear analysis to be performed which allows the local depth of the granular layer to vary by $O(1)$ amounts even when the pattern amplitude is small. The weakly nonlinear analysis and numerical computations provide a robust possible explanation of past experimental results.

Key words. homoclinic snaking, pattern formation, bifurcation, oscillon

AMS subject classifications. 34C37, 34E13, 35B32, 76T25

DOI. 10.1137/090762865

1. Introduction.

It has long been recognized that many externally driven and internally dissipative physical systems spontaneously form patterns with lengthscales determined by balances between physical processes taking place in the bulk of the medium rather than by the precise experimental boundary conditions used. Many examples of such systems are given in the review by Cross and Hohenberg [12], the more recent article by Aranson and Tsimring [1], and the books by Hoyle [21] and Pismen [27]. In the case that such pattern-forming instabilities are supercritical, one expects an almost regular domain-filling structure to arise. The selection between different planforms is necessarily due to nonlinear effects, and progress can be made in many cases through weakly nonlinear analysis near the onset of the instability.

In the case that the pattern-forming instability is subcritical, bifurcation-theoretic results in one space dimension [22, 33] indicate that generically one should expect localized states to arise as well as small-amplitude unstable patterned solutions. Although such localized states are also unstable near the pattern-forming instability, they persist to finite amplitude and can become stable over an open region of parameter space. The overall typical bifurcation structure observed is known as "homoclinic snaking" and persists to a great extent even in finite domains [4, 15].

Detailed results for the Swift–Hohenberg equation, often proposed as a canonical model equation for pattern formation, have been given by many authors, including Sakaguchi and Brand [29], Crawford and Riecke [11], Hiraoka and Ogawa [20], and Burke and Knobloch [6,

*Received by the editors June 23, 2009; accepted for publication (in revised form) by M. Silber December 22, 2009; published electronically March 12, 2010. This research was supported by the Royal Society.
http://www.siam.org/journals/siads/9-1/76286.html
†Department of Mathematical Sciences, University of Bath, Claverton Down, Bath BA2 7AY, UK (jhpd20@bath.ac.uk). This author currently holds a Royal Society University Research Fellowship.
‡Department of Applied Mathematics and Theoretical Physics, University of Cambridge, Wilberforce Road, Cambridge CB3 0WA, UK (sarah.l.lilley@googlemail.com).

7]. In variational systems (of which Swift–Hohenberg is an example) a central part of our understanding of the existence of stable localized states over intervals in parameter space near the "Maxwell point" is given by the locking, or "pinning," that arises between the short lengthscale of the pattern and the long lengthscale of the modulating envelope. The analysis of these pinning effects demands intricate calculations of the exponentially small terms in the weakly nonlinear analysis. Such calculations for the one-dimensional Swift–Hohenberg equation have been carried out recently by Kozyreff and Chapman [23, 8], although the corresponding qualitative geometrical insights were identified by several earlier authors [28, 3, 10].

Renewed recent interest in the mathematical structure of localized states in pattern-forming systems has also resulted in the reconsideration of past experimental work where localized states were observed. This paper is motivated in particular by experimental observations of "oscillons" in large-aspect-ratio circular layers of sinusoidally vertically vibrated material. Umbanhowar, Melo, and Swinney [31] investigated pattern formation in a layer of granular material (bronze spheres of diameter approximately 0.15–0.18mm). In such an experiment the primary control parameters are the frequency of vertical oscillation f (typically in the range 10–40Hz) and nondimensional acceleration $\Gamma = 4\pi^2 A f^2/g$, where the vertical displacement of the layer is given by $z = A\sin 2\pi f t$ and g is the usual gravitational acceleration. As Γ is increased, an initially flat layer undergoes a pattern-forming instability, producing standing-wave patterns of squares (at lower frequencies) or stripes (at higher frequencies) which oscillate subharmonically with respect to the driving frequency. In both cases there is substantial hysteresis, indicating a subcritical bifurcation.

For intermediate frequencies $20 < f < 35$Hz, Umbanhowar, Melo, and Swinney [31] reported the existence of stable localized states, which they called oscillons, in a region of the (f, Γ) plane far below the linear instability to periodic patterns (either stripes or squares). These oscillons took the form of a radially symmetric subharmonically oscillating heap of grains; after one cycle of the driving frequency the heap becomes a crater in the surface of the granular layer, and after two cycles of the driving frequency the heap is reformed. Detailed observations indicated that oscillons are formed in the bulk of the medium rather than by boundary effects and are long-lived coherent structures [31]. Interestingly, the authors observed oscillons with a diameter typically of 30 particles extending up to a maximum height of around 15 particles in a layer of uniform depth (when at rest) of 17 particles. These observations indicate that the local disturbance to the layer height near an oscillon is an $O(1)$ effect; in the bottom of a crater the layer height is reduced to one third, or perhaps even less, of its value in the undisturbed parts of the layer away from the oscillon.

Oscillon states in vertically vibrated fluid, rather than granular, layers were observed by Lioubashevski and coworkers [24, 25]. In the second of these two papers the working fluid used was a non-Newtonian colloidal suspension of clay particles. The regime diagram in the (f, Γ) plane is qualitatively very similar to that measured by [31] in the granular case in that the pattern-forming instability is markedly subcritical, and the oscillons exist, in both cases, in a region that is even more subcritical than the region of stable finite-amplitude patterns. That is, at the linear instability the system jumps rapidly to a finite-amplitude pattern which persists as the forcing is reduced (Γ decreases), but then there is a clear lower stability boundary for the patterned state below which it does not persist, but below which oscillons are stable.

There is another boundary, at even lower forcing, below which the oscillons can no longer persist, but this is clearly distinct from the lower boundary of the existence region of the patterned states. In terms of the usual, Swift–Hohenberg-based, picture of the formation of localized states, this presents a serious difficulty, in that localized states are usually anticipated to persist over an interval of parameter values that contains the Maxwell point of the system, and both the Maxwell point and the whole interval of parameter values over which localized states exist are found to lie above the saddle-node bifurcation point at which the patterned state turns around and restabilizes, not below it. In this paper we investigate a resolution of this apparent contradiction.

Given the difficulty in constructing accurate continuum models for granular media, the proposition of phenomenological equations such as those used by Tsimring and Aranson [30] and Winterbottom, Cox, and Matthews [32] is an entirely reasonable modeling approach. Our aim in this paper is to show that it is possible to extend the analysis carried out by these authors to allow the layer height to vary by large (i.e., order unity) amounts within a weakly nonlinear framework. This approach enables us to attempt a mathematical description of localized states for a model equation for oscillons that nevertheless reconciles the requirements of analyzing dynamics near the pattern-forming instability, but where the layer height undergoes large spatial variations. The phenomenological approach has similarities with the work of Eggers and Riecke [17], who determined a pair of model equations constructed on more physical grounds and showed numerically that an oscillon solution existed. We suspect that a detailed study of the Eggers–Riecke model would show a bifurcation structure similar to that of the model we consider here.

The structure of the paper is as follows. In section 2 we introduce the phenomenological model proposed by Tsimring and Aranson [30] and summarize the asymptotic scalings introduced by Winterbottom, Cox, and Matthews [32] in their analysis. This provides a useful point of contrast with the scalings we employ. In section 3 we set out the details of our alternative weakly nonlinear analysis, which leads to a novel Ginzburg–Landau-like equation that captures more details of the nonlinear terms. The results of numerical investigations of the original Tsimring–Aranson model are presented in section 4. Section 5 concludes.

2. Model equations. Tsimring and Aranson [30] proposed that pattern formation in a vertically vibrated (granular) medium could be described by two local scalar variables: the height of the free surface $H(x,y,t)$ and the local density $\rho(x,y,t)$. The height $H(x,y,t)$ oscillates subharmonically in the instability and so can be written as $H = \psi(x,y,t)\mathrm{e}^{\mathrm{i}\pi ft} +$ c.c., introducing the complex-valued order parameter ψ, and where (here and subsequently) c.c. denotes the complex conjugate. After making simplifying assumptions concerning the coupling between ψ and ρ, they are led to the following pair of coupled PDEs:

$$\psi_t = \gamma\bar{\psi} - (1 - \mathrm{i}\omega)\psi + (1 + \mathrm{i}b)\nabla^2\psi - \psi|\psi|^2 - \rho\psi, \tag{2.1}$$

$$\rho_t = \alpha\nabla\cdot(\rho\nabla|\psi|^2) + \beta\nabla^2\rho. \tag{2.2}$$

The amplitude equation (2.1) for ψ is well known to describe pattern formation in systems which form dispersive waves when they are subjected to parametric forcing; see [9, 5] and references therein. Conservation of mass implies that the PDE for ρ must take the form of a conservation law. The terms on the right-hand side of (2.2) describe the ejection of particles

from more active regions and the local diffusion of particles, respectively. The coupling term $-\rho\psi$ in (2.1) describes, in as simple a form as possible, the damping effect that an increase in the local density has on the initial instability. As Tsimring and Aranson [30] discuss, this term is more generally of the form $-g(\rho)\psi$ for some function $g(\rho)$ that saturates at large ρ. They remark that taking $g(\rho)$ to be linear is appropriate for the case of thin granular layers which we will consider here.

We suppose that the initial state with $\psi \equiv 0$ has a constant layer density $\rho = \rho_0$. The real parameter γ represents the strength of the external periodic forcing, and we will use γ as our primary bifurcation parameter; the trivial solution $\psi = 0$, $\rho = \rho_0$ is linearly stable when γ is sufficiently negative. We suppose implicitly that (2.1)–(2.2) are to be solved in a finite spatial domain with periodic boundary conditions on ψ and ρ. The choice of boundary conditions (within reason) is not expected to unduly influence the formation of localized states, although it may affect some of the details of the bifurcation diagrams [15].

In this paper we will restrict our analysis to one space dimension: this is sufficient to contrast the present approach with previous work. We will leave consideration of axisymmetric, or indeed fully two-dimensional, structures to be the subject of future work. Our analysis of steady states ($\partial/\partial t \equiv 0$) of (2.1)–(2.2) restricted to one space dimension begins by integrating (2.2) to obtain

$$\rho(x) = K \exp\left(-\frac{\alpha}{\beta}|\psi|^2\right).$$

The constant K can be determined from the conservation of ρ. Denoting the spatial average of a function $f(x)$ by $\langle f(x)\rangle \equiv \frac{1}{L}\int_0^L f(x)dx$, we have

$$\rho_0 = \langle \rho(x)\rangle = K\left\langle \exp\left(-\frac{\alpha}{\beta}|\psi|^2\right)\right\rangle,$$

and hence, eliminating K, we have

$$\rho(x) = \rho_0 \frac{\exp\left(-\frac{\alpha}{\beta}|\psi|^2\right)}{\left\langle \exp\left(-\frac{\alpha}{\beta}|\psi|^2\right)\right\rangle}. \tag{2.3}$$

So one-dimensional steady states of (2.1)–(2.2) are identical to steady states of the single nonlocal ODE

$$0 = \gamma\bar{\psi} - (1 - \mathrm{i}\omega)\psi + (1 + \mathrm{i}b)\psi_{xx} - \psi|\psi|^2 - \rho_0\psi\frac{\exp\left(-\frac{\alpha}{\beta}|\psi|^2\right)}{\left\langle \exp\left(-\frac{\alpha}{\beta}|\psi|^2\right)\right\rangle}. \tag{2.4}$$

It is straightforward to investigate steady solutions of (2.4) using the continuation package AUTO [16]. We solve (2.4) as a boundary-value problem in a finite domain of length $L = 32\pi$ with periodic boundary conditions. Figure 1 shows the resulting bifurcation diagram for typical parameter values; the solution measure on the vertical axis is defined to be

$$N_2 = \left(\frac{1}{L}\int_0^L |\psi|^2 + |\psi_x|^2\, dx\right)^{1/2}.$$

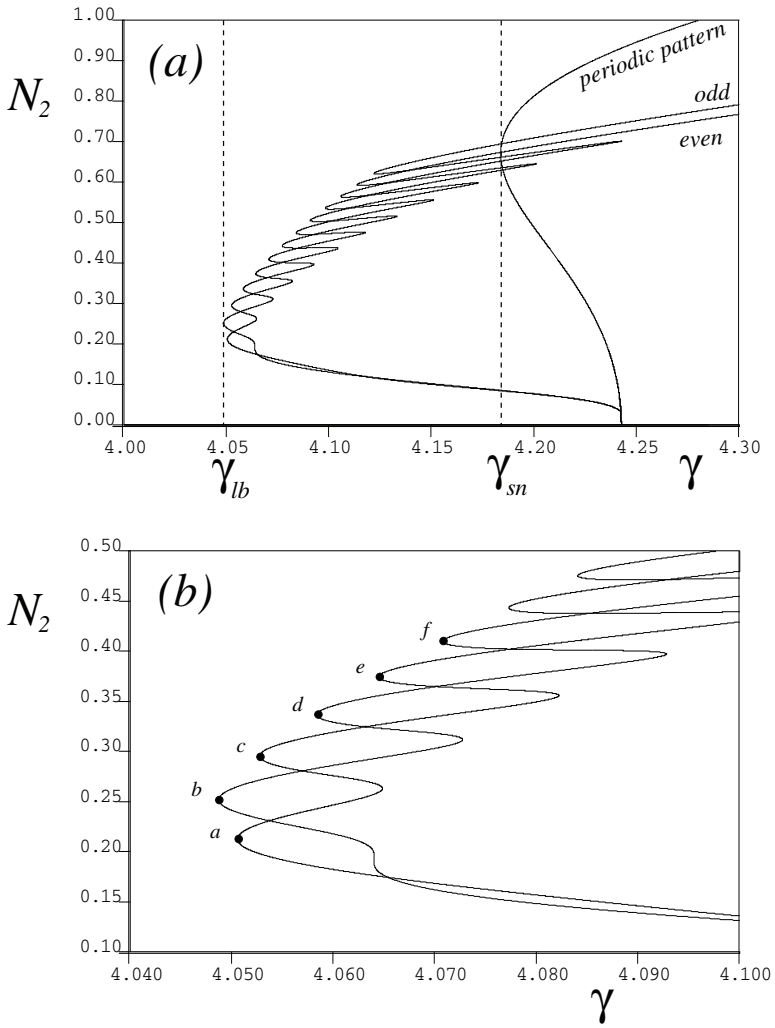

Figure 1. *Typical snaking bifurcation diagram for* (2.4) *showing the spatially periodic pattern branch which bifurcates at lowest* γ*, and the two intertwining branches of localized states, which bifurcate from it. Stability is not indicated.* (a) *The pattern branch stabilizes at a saddle-node bifurcation at* γ_{sn}*, and the branches of localized states exist for* γ *well below* γ_{sn}*.* (b) *is an enlargement of* (a) *showing the usual intertwining bifurcation curves associated with homoclinic snaking. Parameter values are* $\alpha = \omega = 4$*,* $b = \beta = \rho_0 = 1$*, domain size* $L = 32\pi$*, using periodic boundary conditions.*

Figure 1(a) shows the location of the periodic pattern branch that bifurcates first as the driving parameter γ increases. For the parameter values of Figure 1 this pattern-forming instability is subcritical, and the initially unstable periodic branch turns around in a saddle-node bifurcation at γ_{sn} and becomes stable at larger amplitude. Due to finite domain size effects, the two branches of modulated patterns do not bifurcate from $\psi = 0$ at exactly $\gamma_c = 3\sqrt{2}$, but emerge in a secondary bifurcation from the periodic pattern branch. The two branches correspond to odd-symmetric and even-symmetric states, in agreement with symmetry arguments [15]

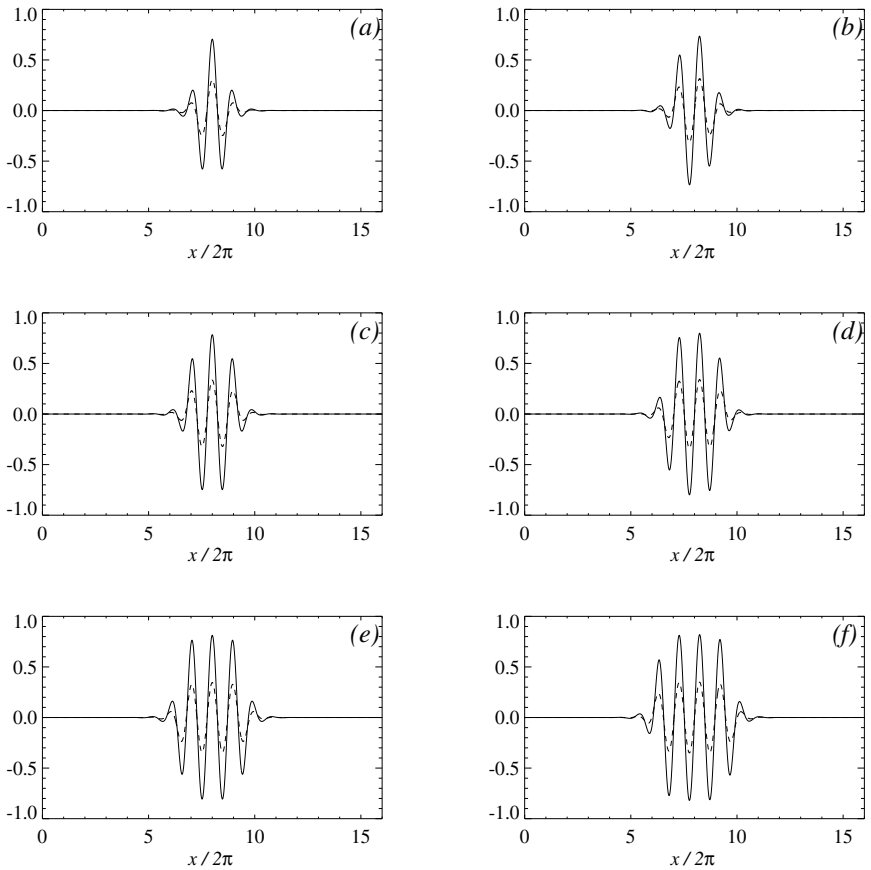

Figure 2. *Steady-state solution profiles at the saddle-node points* a–f *indicated in Figure* 1(b). *Solid and dashed lines give the real and imaginary parts of* ψ*, respectively.*

and exponential asymptotics [23, 8]. Localized solution profiles are shown in Figure 2 at the saddle-node points a–f indicated in Figure 1(b). Timestepping the PDEs (2.1)–(2.2) confirms, as in investigations of the Swift–Hohenberg equation and its extensions [6, 14], that the localized states are stable on the parts of the curves in Figure 1 that have a positive gradient. We anticipate that cross-link ("ladder") branches of asymmetric states connect the odd-symmetric and even-symmetric branches, as has been observed numerically for the Swift–Hohenberg equation [6, 15]. This is argued to be the case on general bifurcation-theoretic grounds by Beck et al. [2].

2.1. Linear and weakly nonlinear analysis. We now briefly summarize the linear stability of the state $\psi = 0$ before turning to weakly nonlinear analysis. To determine the linear stability it is enough to set $\rho = \rho_0$ and, writing $\psi = U + \mathrm{i}V$, we take real and imaginary parts of the linearized version of (2.1). We obtain

$$\frac{\partial}{\partial t}\begin{pmatrix} U \\ V \end{pmatrix} = \tilde{\mathcal{L}}\begin{pmatrix} U \\ V \end{pmatrix} \equiv \begin{pmatrix} (\gamma-1)U - \omega V + U_{xx} - bV_{xx} - \rho_0 U \\ \omega U - (\gamma+1)V + bU_{xx} + V_{xx} - \rho_0 V \end{pmatrix}.$$

Substituting $(U,V)=(U_0,V_0)\mathrm{e}^{\sigma t+\mathrm{i}kx}$ in the usual fashion, we observe that if $\omega b-1-\rho_0<0$, then the most dangerous mode is $k=0$, and instability occurs at $\gamma_0=\sqrt{\omega^2+(1+\rho_0)^2}$. In the present situation we will concentrate on the alternative case, where ω is sufficiently large so that $\omega b-1-\rho_0>0$ and therefore the most unstable mode has a nonzero wavenumber k_c and critical parameter value γ_c given by

$$k_c^2=\frac{\omega b-1-\rho_0}{1+b^2}\qquad\text{and}\qquad\gamma_c=\frac{\omega+(1+\rho_0)b}{\sqrt{1+b^2}}. \tag{2.5}$$

It can be easily verified that $\gamma_0\geq\gamma_c$ with equality only at the codimension-two point $\omega_{CT}=(1+\rho_0)/b$, $\gamma_{CT}=(1+\rho_0)\sqrt{1+b^2}/b$.

The most natural weakly nonlinear calculation to perform to determine the nature of this instability is to fix the values of ω, b, α, β, and ρ_0. We write

$$\gamma=\frac{\omega+(1+\rho_0)b}{\sqrt{1+b^2}}+\varepsilon^2\gamma_2,\qquad X=\varepsilon x,$$

set $\partial/\partial t\equiv 0$, and expand ψ in powers of ε by writing

$$\begin{pmatrix}U\\V\end{pmatrix}=\varepsilon\begin{pmatrix}U_1\\V_1\end{pmatrix}+\varepsilon^2\begin{pmatrix}U_2\\V_2\end{pmatrix}+\varepsilon^3\begin{pmatrix}U_3\\V_3\end{pmatrix}+\cdots.$$

On substitution into (2.4) at $O(\varepsilon)$ we obtain the solution

$$\begin{pmatrix}U_1\\V_1\end{pmatrix}=\begin{pmatrix}c\\1\end{pmatrix}A(X)\mathrm{e}^{\mathrm{i}k_cx}+\text{c.c.},$$

where for convenience we define the coefficient $c=b+\sqrt{1+b^2}$ and as usual introduce the amplitude $A(X)$ whose behavior is determined by a solvability condition obtained at higher order. The solution at $O(\varepsilon^2)$ is straightforward to obtain. At third order we require contributions from the nonlocal term in (2.4). From (2.3) we obtain

$$\begin{aligned}\rho&=\rho_0\frac{1-\frac{\alpha}{\beta}\varepsilon^2(U_1^2+V_1^2)+O(\varepsilon^3)}{\langle 1-\frac{\alpha}{\beta}\varepsilon^2(U_1^2+V_1^2)+O(\varepsilon^3)\rangle},\\&=\rho_0+\frac{\alpha\rho_0}{\beta}\varepsilon^2\left(\langle U_1^2+V_1^2\rangle-U_1^2-V_1^2\right)+O(\varepsilon^3).\end{aligned}$$

In this expression and what follows below, the interpretation of the average $\langle f\rangle$ is modified to take into account the multiple scales in the expansion. We define

$$\langle f(x,X)\rangle=\frac{k_c}{2\pi L}\int_0^L\int_0^{2\pi/k_c}f(x,X)\;dx\;dX,$$

where $0\leq X\leq L$ is the size of the domain, on the scale of the long variable X.

Hence the leading order nonlinear contribution from $-\rho\psi$ arises at $O(\varepsilon^3)$ and is given by

$$-\varepsilon^3\frac{\alpha\rho_0}{\beta}\begin{pmatrix}U_1\\V_1\end{pmatrix}\left(\langle U_1^2+V_1^2\rangle-U_1^2-V_1^2\right).$$

The complete equation at $O(\varepsilon^3)$ is therefore

$$\tilde{\mathcal{L}}\begin{pmatrix} U_3 \\ V_3 \end{pmatrix} = \begin{pmatrix} -\gamma_2 U_1 - 2U_{2xX} + 2bV_{2xX} + U_1(U_1^2+V_1^2) \\ -\gamma_2 V_1 - 2V_{2xX} - 2bU_{2xX} + V_1(U_1^2+V_1^2) \end{pmatrix} + \frac{\alpha\rho_0}{\beta}\begin{pmatrix} U_1 \\ V_1 \end{pmatrix}\left(\langle U_1^2+V_1^2\rangle - U_1^2 - V_1^2\right). \tag{2.6}$$

By applying the solvability condition, we deduce the amplitude equation for $A(X)$ in the usual way. In practice this amounts to identifying the terms on the right-hand side of (2.6) which contain $\mathrm{e}^{\mathrm{i}k_c x}$ and taking an inner product with the row vector $(-c \;\; 1)$ which is the left (adjoint) eigenvector corresponding to the eigenvalue 0. We obtain the amplitude equation

$$0 = a_0 A_{XX} + \gamma_2 A + 3(\phi-1)(1+c^2)A|A|^2 - 2\phi(1+c^2)A\langle|A|^2\rangle, \tag{2.7}$$

where we introduce the parameter combinations

$$a_0 = \frac{2(1+b^2)(\omega b - 1 - \rho_0)}{b(\omega + b(1+\rho_0))} \qquad \text{and} \qquad \phi \equiv \frac{\alpha\rho_0}{\beta},$$

for notational convenience, following Winterbottom, Cox, and Matthews [32]. This equation corresponds exactly (after a rescaling) to that derived by [32] for stripe patterns. In their analysis they worked with the original system (2.1)–(2.2), expanded ψ as above, and wrote

$$\rho = \rho_0 + \varepsilon^2 C(X,T) + \text{other terms at } O(\varepsilon^2) + O(\varepsilon^3), \tag{2.8}$$

where $T = \varepsilon^2 t$ is a new slow timescale. From solvability conditions at $O(\varepsilon^3)$ and $O(\varepsilon^4)$, respectively, they obtained the coupled amplitude equations

$$A_T = A + A_{XX} - A|A|^2 - AC, \tag{2.9}$$

$$\frac{1}{\sigma}C_T = C_{XX} + \frac{\mu}{\sigma}(|A|^2)_{XX}, \tag{2.10}$$

where $\mu/\sigma = 2\phi/(3-\phi)$. The equivalence of these two calculations can be easily seen: starting from (2.9) and (2.10), one can set $\partial/\partial T \equiv 0$ and integrate (2.10) to obtain

$$C(X) = \frac{2\phi}{3-\phi}\left(\langle|A|^2\rangle - |A|^2\right)$$

and hence obtain the nonlocal amplitude equation

$$0 = A + A_{XX} + \frac{3(\phi-1)}{3-\phi}A|A|^2 - \frac{2\phi}{3-\phi}A\langle|A|^2\rangle,$$

which is equivalent to (2.7) after rescalings of A and X.

Returning to (2.7), we observe that the uniform straight roll pattern has amplitude $|A_0|^2 = \gamma_2/[(3-\phi)(1+c^2)]$ and hence bifurcates supercritically when $0 < \phi < 3$ and subcritically when $\phi > 3$. Moreover, testing for modulational instability by setting $A = A_0(1 + a\mathrm{e}^{\mathrm{i}\ell X})$ (taking

A_0 to be real) indicates that supercritical straight roll patterns (with the critical wavenumber k_c) are unstable to long wavelength modes when $\phi > 1$; in the limit $\ell \to 0$ we obtain

$$0 = a(\gamma_2 + 9(\phi-1)A_0^2 - 2\phi A_0^2) + O(a^2) = a\left(\frac{6(\phi-1)}{3-\phi}\right) + O(a^2), \tag{2.11}$$

showing that the coefficient of the linear term changes sign when ϕ passes through unity. This calculation has a slightly formal nature since, by considering only steady states from the beginning, we have not properly derived the $\partial A/\partial T$ term which would be expected to lie on the left-hand side of (2.7). However, the result is in complete agreement with the analytic and numerical work carried out by [32] on the equivalent (but time-dependent) system (2.9)–(2.10).

Work by Matthews and Cox [26] on systems with conservation laws leads us to suspect that strongly modulated solutions to (2.7) exist, indicating that in large enough domains, localized states might be observed. It is straightforward to see that (2.7) posed on an infinite domain has a family of exact, *sech*-profile solutions given implicitly by

$$A_{loc}(X) = \left(\frac{4\phi(1+c^2)\langle A_{loc}^2\rangle - 2\gamma_2}{3(\phi-1)(1+c^2)}\right)^{1/2} \operatorname{sech}\left(\frac{2\phi(1+c^2)\langle A_{loc}^2\rangle - \gamma_2}{a_0}\right)^{1/2} X. \tag{2.12}$$

After squaring and integrating this solution over $-\infty < X < \infty$, we obtain an explicitly soluble relationship between $\langle A_{loc}^2\rangle$ and γ_2 given by

$$9(\phi-1)^2(1+c^2)^2\langle A_{loc}^2\rangle^2 - 32a_0\phi(1+c^2)\langle A_{loc}^2\rangle + 16a_0\gamma_2 = 0.$$

This expression is valid only when a modulation instability giving rise to solutions of the form (2.12) exists, i.e., when $\phi \geq 1$. In the case $\phi = 1$ the uniform solution $A = A_0$ coincides with the *sech* solution $A = A_{loc}$. For $\phi > 1$ the curve of $A_{loc}(X)$ solutions in the $(\gamma_2, \langle A^2\rangle)$ plane begins in $\gamma_2 > 0$ at small $\langle A^2\rangle$ before moving into $\gamma_2 < 0$ at larger amplitude and remaining there, with $\langle A^2\rangle$ monotonically increasing as γ_2 becomes increasingly negative. In large but finite domains with periodic boundary conditions the *sech* profile is replaced by an elliptic function, and the localized branch bifurcates in a secondary bifurcation from the uniform solution $A = A_0$, but the monotonic increase of $\langle A^2\rangle$ as γ_2 becomes increasingly negative remains.

Overall this behavior is suggestive of the capacity of the original coupled system's ability to sustain localized states, but indicates that within the scalings adopted in this analysis the effects of the nonlinearity are not captured sufficiently well to enable the formation of strongly nonlinear localized states at larger amplitudes. In the next section we will introduce new scalings to produce a novel amplitude equation containing a more complicated nonlocal nonlinearity.

3. The "weak diffusion" limit. The physical intuition behind the formation of localized states discussed in the introduction is extremely similar to the physical mechanisms identified in magnetoconvection which stabilized large-amplitude convection cells even at high magnetic field strengths due to a balance between magnetic flux expulsion from the eddy and diffusion of the magnetic field [13, 14]. A similar physical intuition appears to contribute to the formation of oscillons: localized states are stabilized when the rate of horizontal diffusion of the granular

material is slow compared to the rate of expulsion of material from more active to less active regions of the granular layer. Mathematically this corresponds to taking the ratio α/β to be large. Considering (2.3), the appropriate balance is clearly $\psi \sim \varepsilon$, $\alpha/\beta \sim \varepsilon^{-2}$, so that the full form of the nonlinearity is retained. Hence this limit is one in which the nonlinear rate of expulsion of material balances the diffusion coefficient β, even when the amplitude of the pattern is small. In order to keep the leading order problem tractable, it is therefore necessary to also rescale the coefficient $\rho_0 \sim \varepsilon^2$. This does not introduce a difficulty since the coefficient ρ_0 is only an adjustment to the order unity damping term provided by the real part of the term $-(1-\mathrm{i}\omega)\psi$ in (2.4). By rescaling ρ_0 to be small, we do not alter the qualitative structure of the linear terms.

In summary we propose the scalings

$$\frac{\alpha}{\beta} = \frac{1}{\varepsilon^2}, \qquad \rho_0 = \varepsilon^2 h, \qquad X = \varepsilon x,$$

and recompute the linear and weakly nonlinear analysis of the previous section. As before, we write $\psi = U + \mathrm{i}V$ and expand in powers of ε:

$$\begin{pmatrix} U \\ V \end{pmatrix} = \varepsilon \begin{pmatrix} U_1 \\ V_1 \end{pmatrix} + \varepsilon^2 \begin{pmatrix} U_2 \\ V_2 \end{pmatrix} + \varepsilon^3 \begin{pmatrix} U_3 \\ V_3 \end{pmatrix} + \cdots .$$

At $O(\varepsilon)$ we have the slightly modified linear problem

$$\frac{\partial}{\partial t}\begin{pmatrix} U \\ V \end{pmatrix} = \mathcal{L}\begin{pmatrix} U \\ V \end{pmatrix} \equiv \begin{pmatrix} (\gamma-1)U - \omega V + U_{xx} - bV_{xx} \\ \omega U - (\gamma+1)V + bU_{xx} + V_{xx} \end{pmatrix}.$$

On substituting $(U, V) = (u_0, v_0)\mathrm{e}^{\sigma t + \mathrm{i}kx}$, we find that a pattern-forming instability occurs at $\gamma_* = (\omega + b)/\sqrt{1+b^2}$ with critical wavenumber given by $k_*^2 = (\omega b - 1)/(1+b^2)$. As before, we assume that ω is sufficiently large (i.e., $\omega > 1/b$) that the initial instability is at nonzero wavenumber. We write $\gamma = \gamma_* + \varepsilon^2\gamma_2$ and compute the solutions at $O(\varepsilon)$ and $O(\varepsilon^2)$, which are easily found to be

$$\begin{pmatrix} U_1 \\ V_1 \end{pmatrix} = \begin{pmatrix} c \\ 1 \end{pmatrix} A(X)\mathrm{e}^{\mathrm{i}k_* x} + \text{c.c.},$$

where $c = b + \sqrt{1+b^2}$ as before, and

$$\begin{pmatrix} U_2 \\ V_2 \end{pmatrix} = 2\mathrm{i}k_* \frac{(1+b^2)^{3/2}}{\omega + b} \begin{pmatrix} 0 \\ 1 \end{pmatrix} \left(A_X \mathrm{e}^{\mathrm{i}k_* x} - \bar{A}_X \mathrm{e}^{-\mathrm{i}k_* x} \right).$$

It is enough, in fact, to consider $A(X)$ to be real in what follows, since the instability of the uniform pattern that gives rise to modulated states is amplitude-driven rather than phase-driven. At $O(\varepsilon^3)$ we obtain

$$\mathcal{L}\begin{pmatrix} U_3 \\ V_3 \end{pmatrix} = \begin{pmatrix} -\gamma_2 U_1 - 2U_{2xX} + 2bV_{2xX} + U_1(U_1^2 + V_1^2) + hU_1 \frac{\exp(-U_1^2 - V_1^2)}{\langle \exp(-U_1^2 - V_1^2) \rangle} \\ -\gamma_2 V_1 - 2V_{2xX} - 2bU_{2xX} + V_1(U_1^2 + V_1^2) + hV_1 \frac{\exp(-U_1^2 - V_1^2)}{\langle \exp(-U_1^2 - V_1^2) \rangle} \end{pmatrix},$$

from which we extract an amplitude equation for $A(X)$ by taking an inner product with the row vector $(-c \;\; 1)$ and then multiplying by $(k_*/\pi)\cos(k_* x)$ and integrating over one spatial period $2\pi/k_*$. The resulting amplitude equation takes the form

$$0 = (c^2-1)\gamma_2 A + \frac{4k_*^2(1+bc)(1+b^2)^{3/2}}{\omega+b} A_{XX} - 3(c^2-1)(1+c^2)A^3 + \frac{1}{2}\mathcal{I}(X), \tag{3.1}$$

where $\mathcal{I}(X)$ denotes the contribution from the final terms in the entries in the column vector on the right-hand side:

$$\mathcal{I}(X) = \frac{k_*}{\pi}\int_0^{2\pi/k_*} (1-c^2)2A\cos^2 k_* x \exp[-(1+c^2)4A^2\cos^2 k_* x]K \; dx,$$

where, as previously, we define $K = h/\langle \exp(-\frac{\alpha}{\beta}|\psi_1|^2)\rangle$. We define the rescaled amplitude $B(X) = \sqrt{2(1+c^2)}A$ and observe that the integral can be written more compactly as a derivative with respect to B:

$$\mathcal{I}(X) = \frac{k_*\sqrt{2}(1-c^2)K}{\pi\sqrt{1+c^2}} \int_0^{2\pi/k_c} -\frac{1}{4}\frac{\mathrm{d}}{\mathrm{d}B}\left[\exp\left(-2B^2\cos^2 k_* x\right)\right] \; dx. \tag{3.2}$$

A further simplification can be made by writing $2\cos^2 k_* x = 1 + \cos 2k_* x$ and rescaling the integration variable by writing $y = 2k_* x$. We then obtain

$$\mathcal{I}(X) = \frac{\sqrt{2}(c^2-1)K}{2\pi\sqrt{1+c^2}}\frac{\mathrm{d}}{\mathrm{d}B}\left[\mathrm{e}^{-B^2}\int_0^{\pi}\exp\left(-B^2\cos y\right)\; dy\right].$$

The y-integral is now in a standard form: it is a modified Bessel function of the first kind; see section 8.431 of [19]. More precisely, we have (by definition) that

$$I_0\left(-B^2\right) = \frac{1}{\pi}\int_0^{\pi}\exp\left(-B^2\cos y\right)\; dy$$

is the modified Bessel function of the first kind of order zero. $I_0(z)$ is closely related to the usual Bessel function of the first kind, $J_0(z)$: $I_0(z) = J_0(\mathrm{i}z)$. In contrast to $J_0(z)$, $I_0(z)$ is a monotonically increasing function when z is real. Note that $I_0(-B^2) = I_0(B^2)$ (this can be shown easily by changing the direction of integration by introducing $\tilde{y} = \pi - y$), and that $I_0(0) = 1$. Hence the nonlinear nonlocal term $\mathcal{I}$ can be compactly written as

$$\mathcal{I}(X) = \frac{\sqrt{2}(c^2-1)K}{2\sqrt{1+c^2}}\frac{\mathrm{d}}{\mathrm{d}B}\left[\mathrm{e}^{-B^2}I_0\left(B^2\right)\right].$$

After similar manipulations we have a similarly compact expression for the integral K:

$$K = \frac{h}{\left\langle \mathrm{e}^{-B^2}I_0\left(B^2\right)\right\rangle}.$$

Hence (3.1) can be further tidied up by introducing the rescaled amplitude $B(X)$ which results in the amplitude equation

$$0 = \gamma_2 B + a_1 B_{XX} - \frac{3}{2}B^3 + h\frac{\frac{\mathrm{d}}{\mathrm{d}B}\left[\mathrm{e}^{-B^2}I_0(B^2)\right]}{2\left\langle \mathrm{e}^{-B^2}I_0(B^2)\right\rangle}, \tag{3.3}$$

where the coefficient $a_1 = 2(1+b^2)(\omega b - 1)/[b(\omega+b)]$.

3.1. Small-amplitude periodic and localized states. Although a full analytic study of the solutions of (3.3) is beyond the scope of this paper, we can deduce that it has several features in common with (2.7). At small amplitude, solutions of (3.3) are given approximately by solving

$$0 = a_1 B_{XX} + B(\gamma_2 - h - h\langle B^2\rangle) + \frac{3}{2}(h-1)B^3 + O(B^5).$$

As in the previous section, it is straightforward to examine both the uniform-amplitude and the modulated solutions of this equation. Uniform solutions $B = B_0$ satisfy

$$0 = \gamma_2 B_0 - \frac{3}{2}B_0^3 + h\left(-B_0 + \frac{1}{2}B_0^3\right) + O(B_0^5),$$

indicating that, similar to (2.7), the bifurcation to spatially periodic states is supercritical if $h < 3$ and subcritical if $h > 3$. On an infinite domain, modulated solutions with a *sech* profile satisfy the implicit relation

$$B_{loc}(X) = \left(\frac{4(h - \gamma_2 + h\langle B_{loc}^2\rangle)}{3(h-1)}\right)^{1/2} \operatorname{sech}\left(\frac{h - \gamma_2 + h\langle B_{loc}^2\rangle}{a_1}\right)^{1/2} X.$$

After squaring and integrating, as before, we obtain the quadratic relation

$$9(h-1)^2\langle B_{loc}^2\rangle^2 - 64a_1 h\langle B_{loc}^2\rangle + 64a_1(\gamma_2 - h) = 0.$$

In the special case $h = 1$ we again see that the uniform solutions coincide with the *sech* ones. When $h > 1$ we can compute that the curve in the $(\gamma_2, \langle B^2\rangle)$ plane on which $B_{loc}(X)$ solutions exist for small amplitudes exists in $\gamma_2 > h$ before moving into $\gamma_2 < h$ at larger $\langle B^2\rangle$. As noted toward the end of section 2.1, in a finite domain with periodic boundary conditions the *sech* solution is replaced by one which can be written in terms of an elliptic function.

3.2. Larger-amplitude localized states. At larger amplitude the localized states resemble a section of uniform-amplitude spatially periodic pattern confined between two fronts connecting the pattern envelope to the trivial zero state. In this section we derive an approximate form for these wider localized states and show that this approximate expression agrees very well with numerical bifurcation diagrams computed using AUTO.

We begin by observing that the nonlocal amplitude equation (3.3) can be integrated after multiplying through by B_X. This gives the "energy-like" expression

$$E = \frac{\gamma_2}{2}B^2 + \frac{a_1}{2}(B_X)^2 - \frac{3}{8}B^4 + \frac{h}{2}\left[\frac{\exp(-B^2)I_0(B^2)}{\langle \exp(-B^2)I_0(B^2)\rangle} - 1\right], \tag{3.4}$$

where the -1 has been introduced for convenience so that the solution $B(X) \equiv 0$ lies in the set of solutions with $E = 0$. Suppose now that we consider solutions of (3.3) for which the localized state occupies a given fraction ℓ/L of the domain $0 \le X \le L$ and has a constant amplitude $B = B_f$, before dropping rapidly to zero for the remaining part of the domain, of width $L - \ell$. We approximate by assuming that this "wide" localized state has a piecewise

constant amplitude, and ignore terms containing derivatives of B. The integral term in (3.3) can be approximated by

$$\left\langle \mathrm{e}^{-B^2} I_0(B^2) \right\rangle \approx \frac{\ell}{L} \mathrm{e}^{-B_f^2} I_0(B_f^2) + \frac{L-\ell}{L} \;\equiv\; \mathcal{I}_\ell.$$

There are two criteria that must be satisfied in order to construct a wide localized state. First, the value of B_f must satisfy the amplitude equation when the nonlocal term has the value $\mathcal{I}_\ell$, i.e.,

$$0 = \gamma_2 B_f - \frac{3}{2} B_f^3 + \frac{h}{2} \frac{2 B_f \mathrm{e}^{-B_f^2} (I_1(B_f^2) - I_0(B_f^2))}{\mathcal{I}_\ell},$$

where $I_1(z) \equiv I_0'(z)$ is the modified Bessel function of the first kind of order 1. Second, the value of E must be constant along such a solution, i.e., $E|_{B=B_f} = E|_{B=0}$, which implies

$$\frac{\gamma_2}{2} B_f^2 - \frac{3}{8} B_f^4 + \frac{h}{2} \left[\frac{\mathrm{e}^{-B_f^2} I_0(B_f^2)}{\mathcal{I}_\ell} - 1 \right] = \frac{h}{2} \left[\frac{1}{\mathcal{I}_\ell} - 1 \right].$$

Eliminating $h/\mathcal{I}_\ell$ between these two expressions gives a relation between γ_2 and B_f which is, rather surprisingly, "universal" in the sense that it does not depend on any other parameters in the problem:

$$\gamma_2 = \frac{\frac{3}{2} B_f^2 \left[\mathrm{e}^{B_f^2} + \frac{1}{2} B_f^2 I_1(B_f^2) - (1 + \frac{1}{2} B_f^2) I_0(B_f^2) \right]}{\mathrm{e}^{B_f^2} + B_f^2 I_1(B_f^2) - (1 + B_f^2) I_0(B_f^2)} \;\equiv\; \mathcal{F}(B_f^2). \tag{3.5}$$

For small B_f we can derive an intuitive feel for the function $\mathcal{F}(B_f^2)$ by computing its Taylor series:

$$\mathcal{F}(B_f^2) = 1 + \frac{10}{9} B_f^2 + \frac{115}{1296} B_f^4 + \frac{349}{116640} B_f^6 - \frac{25567}{8398080} B_f^8 - \frac{57859}{211631616} B_f^{10} + O(B_f^{12}).$$

It turns out that the above approximation is numerically very useful: it is accurate to better than 0.01% for the $O(1)$ values of B_f that arise for typical parameter values used in numerical simulation.

The function $\mathcal{F}(B_f^2)$ defines the "Maxwell curve" for the system where a solution consisting of a localized active state of length ℓ, along with a higher material density outside this active region, has the same energetic value as the trivial state. It therefore should give a prediction of where localized states should be found. Figure 3 compares the curve (3.5) with solutions of the amplitude equation (3.3) and shows that it correctly predicts the location of the upper half of the curve of localized states, when the localized states have become broad enough to be accurately represented by the piecewise constant ansatz proposed just after (3.4) above. Numerical results indicate that shorter localized states always exist underneath and to the right of the Maxwell curve since they must reconnect to the uniform solution near $\gamma_2 = h > 3$. Although we have not ruled out their existence in $\gamma_2 < 1$, we do not observe this numerically

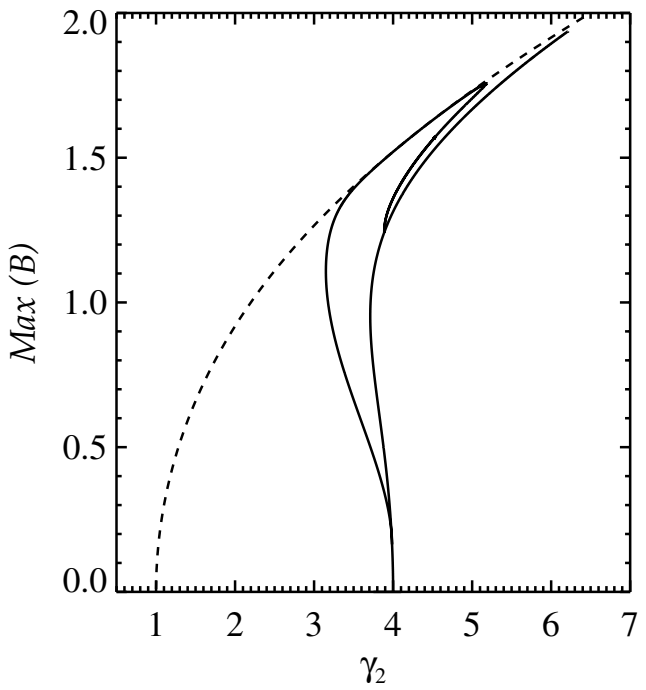

Figure 3. *Comparison of the "universal" Maxwell curve* (3.5) *(dashed line) with solutions of* (3.3) *(solid lines). The constant solution of* (3.3) *represents the spatially periodic pattern and bifurcates subcritically. As in Figure* 1*, the branch of localized states bifurcates from this branch at small amplitude and extends further to the left (i.e., it is more subcritical). The agreement between the location of the larger-amplitude localized states and the Maxwell curve is excellent. Parameters are* $\omega = h = 4$, $b = 1$. *Domain size* $0 \le X \le 20$, *with periodic boundary conditions.*

and propose that $\gamma_2 = 1$ provides a lower bound on the location of the center of the snaking curve. Transforming $\gamma_2 = 1$ back into the original unscaled variables implies a lower bound $\gamma_{min} = \gamma_* + \beta/\alpha$. This estimate, of course, cannot take into account the width of the snaking region which arises through pinning between the periodic pattern and its envelope. Therefore it is not directly an estimate of γ_{lb}, although it is useful to make this comparison; see Figure 4. For the parameter values used in Figure 1 we have $\gamma_{min} = 5/\sqrt{2} + 1/4 \approx 3.685$, which is consistent with the observed location of the snaking in Figure 1. Given this expression for γ_{min}, we might expect the location γ_{lb} of the left-most saddle-node bifurcation on the snaking curve to follow a similar scaling $\gamma_{lb} - \gamma_* \sim \alpha^{-1}$. This scaling is confirmed by Figure 4, which indicates that γ_{lb} does indeed approach γ_* in this way, in the limit $\varepsilon \to 0$. Comparisons between the curves in Figure 4 for domain sizes $L = 24\pi, 32\pi, 64\pi$ indicate that the deviation of the slope from -1 at large α appears to be due to finite domain size effects: at large α the localized states at γ_{lb} become broader and can be correctly captured only in increasingly large domains.

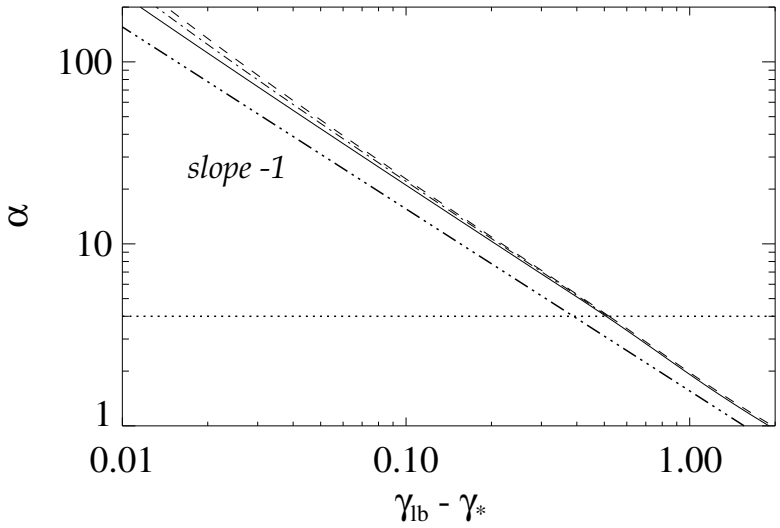

Figure 4. *Location of the left-most saddle-node bifurcation γ_{lb} on the snaking curve for (2.4) as α increases (solid line), in the limit $\varepsilon \to 0$, setting $\rho_0 = 4/\alpha$ so that $\alpha\rho_0/\beta = 4$ is kept constant, as is required for the "weak diffusion" limit. Curves for three domain sizes are shown: $L = 24\pi$ (dashed), $L = 32\pi$ (dash-dotted), and $L = 64\pi$ (solid). The dash-triple-dotted line is the curve $\gamma_{min} = \gamma_* + \beta/\alpha$, which has slope -1, for comparison. The horizontal dotted line indicates $\alpha = 4$, used in Figures 1 and 2. Other parameter values are $\omega = 4$, $b = \beta = 1$.*

4. Numerical results. In this section we discuss a brief selection of numerical results which illustrate how the localized states evolve as first γ and then ω is varied. We then present, in section 4.3, numerical results showing that the turns in the homoclinic snaking curves disappear in some parameter regimes, although the localized states persist; we refer to this novel behavior as "smooth snaking."

4.1. Further up the snaking curves. Although the discussion above indicates that localized states appear well below the saddle-node bifurcation on the periodic pattern branch at $\gamma = \gamma_{sn}$ (see Figure 1) when $\omega = 4$, it is clearly of substantial interest to try to see how the bifurcation structure evolves away from $\omega = 4$. This is in general a complex issue, which is discussed in detail elsewhere for simpler pattern-forming systems; for example, the change in the most unstable wavenumber (2.5) as ω varies not only gives rise to changes in the order and locations in which periodic pattern branches bifurcate from the trivial solution $\psi = 0$, but also affects the snaking structure and how it may, in a finite domain, reconnect with the periodic branches at large amplitude [4, 15]. In fact, in the present case this reconnection is not always observed: for the parameter values of Figure 1 the localized states develop kinks which fill the domain outside the localized state, as shown in Figure 5. It is striking that the wavelength within the localized states in Figure 5 increases rapidly as we move away from the snake. Figure 5(d) shows the development of a kink outside the original localized state. As a result of the kink, the density $\rho(x)$ in the quiescent region near the endpoints of the domain

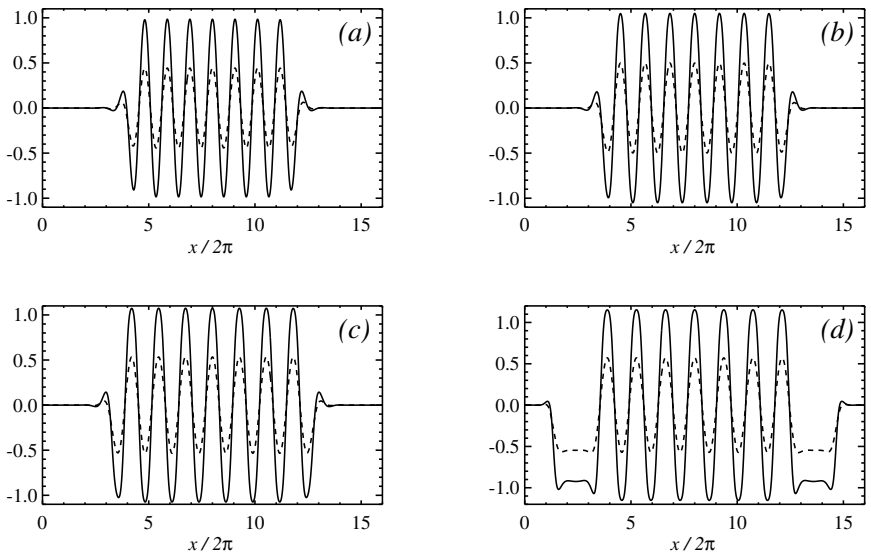

Figure 5. *Evolution of the localized states as γ increases, above the snaking regime, near the labels odd and even in Figure 1*(a). *Parameters are* (a) $\gamma = 4.243$, (b) $\gamma = 4.3434$, (c) $\gamma = 4.408$, (d) $\gamma = 4.559$. *For all plots* $\alpha = \omega = 4$, $b = \beta = \rho_0 = 1$, *domain size* $L = 32\pi$ *with periodic boundary conditions. Solid and dashed lines indicate the real and imaginary parts of* $\psi(x)$, *respectively.*

has an unphysically high value. We have not investigated the stability of these states; even if they are stable within the model (2.1)–(2.2) they are highly unlikely to be relevant to the interpretation of experimental results.

4.2. Evolution as ω varies. Figure 6 plots the continuation in ω of a number of key bifurcation curves in an attempt to convey the region of existence of the localized states shown in Figures 2 as ω moves away from $\omega = 4$.

Near $\omega = 4$ we see that the curves of saddle-node bifurcations on the snake remain almost horizontal, and far below γ_{sn}. Even though γ_{sn} refers only to the saddle-node on a single one of the many branches of periodic patterned states (it corresponds to the branch that bifurcates first as γ increases for $\omega = 4$), experience suggests that saddle-nodes on the other periodic branches will extend by similar amounts into values of γ below the linear instability at γ_c. Thus, over a range of ω, periodic patterns are stable down to $\gamma - (\omega + (1+\rho_0)b)/(1+b^2)^{1/2} \approx -0.06$, while localized states are stable below this, down to $\gamma - (\omega + (1+\rho_0)b)/(1+b^2)^{1/2} \approx -0.2$. Hence the model equations (2.1)–(2.2) are capable of generating the clear separation of localized and patterned regimes seen experimentally in the papers discussed in section 1.

As ω decreases, the location in γ of the left-most saddle-node bifurcations in Figure 1 decreases, following the linear stability boundary $\gamma_c(\omega)$. As the most unstable wavenumber k_c associated with $\gamma_c(\omega)$ decreases, it is not surprising that the wavenumber within the localized states also decreases dramatically, as shown in Figure 7. Such wide, almost domain-filling, localized states are unlikely to have physical relevance for the same reason as those states higher up the snake, discussed in section 4.1; the density $\rho(x)$ outside the localized state becomes

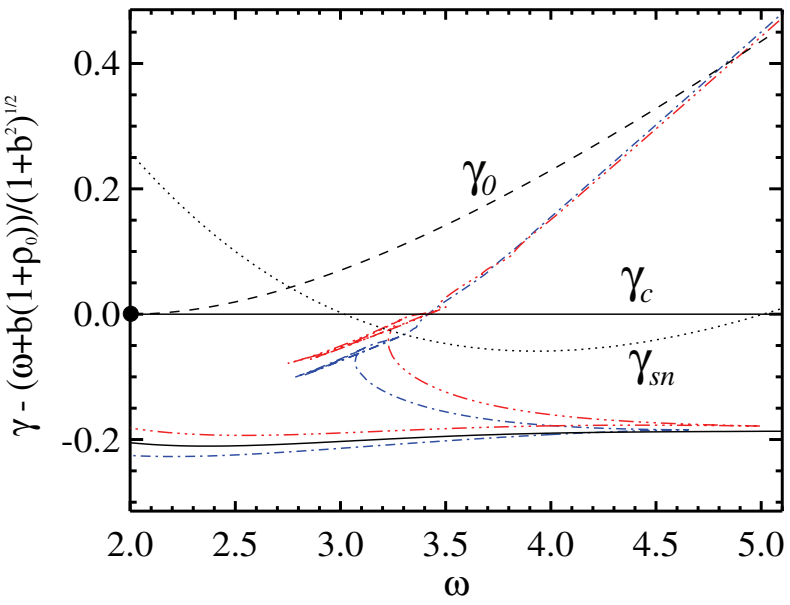

Figure 6. *Continuation of bifurcation curves in the* $(\omega, \gamma - (\omega + (1+\rho_0)b)/(1+b^2)^{1/2})$ *plane. Along the dashed curve* γ_0 *the trivial state is unstable to perturbations with zero wavenumber. Along the solid curve* γ_c *given by* (2.5(b)) *the trivial state first becomes unstable to nonzero wavenumber perturbations as* γ *is increased. The black dot marks the codimension-two point* $\omega = \omega_{CT}$, $\gamma = \gamma_{CT}$ *where these curves intersect. The dotted curve* γ_{sn} *marks the location of the saddle-node bifurcation on the periodic branch for the wavenumber which is most unstable for* $\omega = 4$. *Other solid and dash-dotted curves indicate the evolution of the location of saddle-node bifurcations from the three saddle-node bifurcations labeled* a *(blue dash-dotted line),* c *(black solid line), and* e *(red dash-triple-dotted line) in Figure* 1(b), *whose profiles are shown in the corresponding parts of Figure* 2. *Other parameters are* $\alpha = 4$, $b = \beta = \rho_0 = 1$, *with a domain size* $L = 32\pi$ *and periodic boundary conditions.*

unphysically large, an order of magnitude greater than that inside the layer. Continuation of these localized states in γ indicates that they grow not by the addition of further periods of a periodic pattern, but by developing kinks, producing solutions similar to Figure 5(d). The development of these kinks also produces the rather wild meandering of the saddle-node curves seen in the vicinity of the point $(3.2, 1.35)$ in Figure 6. As these saddle-node curves (at finite amplitude) move into the region above γ_c, they fill the domain and hence become physically irrelevant. We have not determined their ultimate fate, which appears to depend sensitively on the domain size.

As ω increases above $\omega = 4$, we find that many of the saddle-node bifurcations disappear in cusp bifurcations (for example, at the point $(5.0, -0.18)$ in Figure 6). This is indicative of a "smoothing out" of the snaking curves in a manner very similar to that to which we will turn our attention in the following section.

4.3. Smooth snaking. One of the major effects of the nonlocal term in (2.4) is to introduce a tilt to the usual homoclinic snaking bifurcation diagram. Without a nonlocal term, for example in the quadratic-cubic or cubic-quintic Swift–Hohenberg equation, the saddle-node

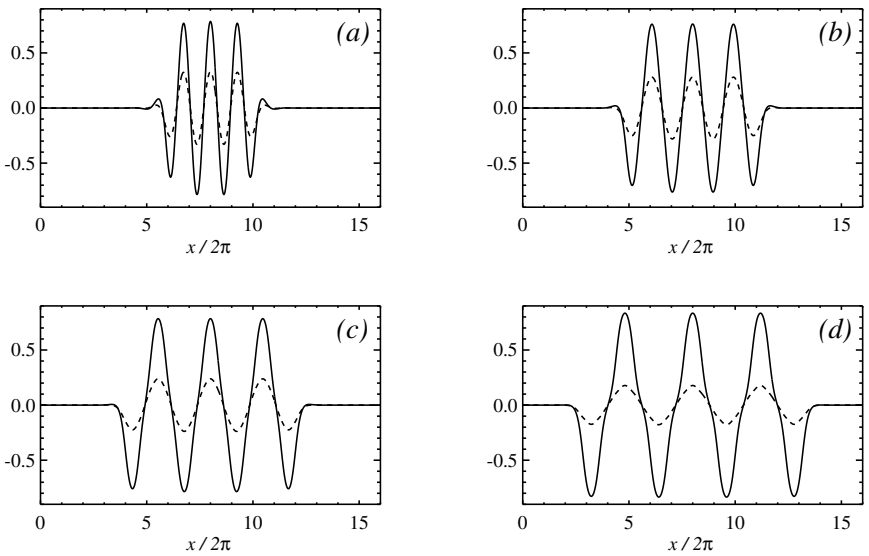

Figure 7. *Evolution of the localized state shown in Figure 2(e) at its saddle-node point as ω is decreased from $\omega = 4.0$.* (a) $\omega = 3.0$, (b) $\omega = 2.0$, (c) $\omega = 1.5$, (d) $\omega = 1.0$. *Solid and dashed lines indicate the real and imaginary parts of $\psi(x)$, respectively.*

bifurcations on successive turns of the snake are aligned vertically and asymptote to limiting values which correspond to the boundary of a region where a front between the patterned state and the trivial state is pinned and held stationary.

With a nonlocal term, the snake tilts because, as the width of the localized state increases, the background state also evolves since it collects the material expelled from the localized active region. As the influence of the snake width on the background state (i.e., the coefficient of the nonlinear coupling term in (2.2)) increases, one might conjecture that the snake becomes tilted and distorted further, until, with extreme tilting, the saddle-node bifurcations on the snaking curves disappear in pairs at cusp points, leading to a monotonic snaking curve without saddle-node bifurcations. Although this behavior was not found in previous work [18, 14] on an extension of the Swift–Hohenberg equation that gave rise to tilted (or "slanted") snaking, it does arise in this problem; see Figure 8.

Clearly, as α increases, the left-hand endpoint of the snake moves to lower amplitude and into a weakly nonlinear regime. Figure 9 shows the smooth evolution of the localized state along the branch shown in Figure 8. Figure 10 shows, in a different limit with h kept fixed as α increases, that the saddle-nodes disappear in cusp bifurcations one-by-one as α increases; they are independent bifurcation events. In this limit the location of the left-most saddle-node bifurcation appears to scale as $\gamma_{lb} - \gamma_* \sim \alpha^{-1/2}$, rather than $\sim \alpha^{-1}$ as in Figure 4. It makes sense physically that the weakly nonlinear limit is approached more slowly in this case since we are increasing only the coefficient α of the "material expulsion" term in (2.2) without simultaneously decreasing the average density ρ_0 of the layer which is an additional effect that reinforces the effects of any absolute fluctuation in spatial density.

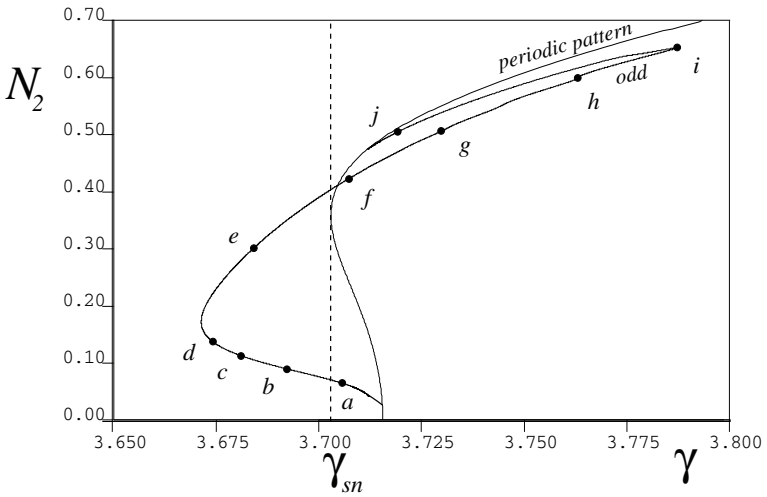

Figure 8. *Bifurcation diagram in a "smooth snaking" regime. Branches of localized states bifurcate at small amplitude from the spatially periodic pattern and exist for γ below γ_{sn} as in Figure 1. (Only the branch of odd-symmetric states is shown here.) The branch reconnects to the periodic pattern at large amplitude and is composed entirely of localized states, but contains only two saddle-node bifurcations. The solutions at labels* a–j *are shown in the corresponding parts of Figure 9. Parameters are $\omega = 4$, $b = \beta = 1$, $\alpha = 16$, and $\rho_0 = 0.25$ so that, as in Figure 1, $h = 4$. The domain size is $L = 32\pi$, and periodic boundary conditions are imposed.*

5. Discussion. In this paper we have provided a detailed analysis of model equations proposed by Tsimring and Aranson [30] relevant to experimental work on layers of vertically vibrated granular material [31] and non-Newtonian fluid [24, 25]. We introduced a novel distinguished limit in order to derive a new amplitude equation for the weakly nonlinear pattern-forming behavior. This new amplitude equation is of Ginzburg–Landau type but with a considerably more complicated, nonlocal, nonlinear term. The new amplitude equation captures the behavior of the system over a wider region of parameter space than the traditional scalings, and provides insight into the role played by the conservation law for the material in sustaining localized states over a much wider range of forcing parameters than is usually the case in such subcritical pattern-forming problems.

Our major conclusion is that even a weak coupling to a second field variable obeying a conservation law dramatically enhances localization and enables oscillons to persist in a region of parameter space below the lower limit of periodic domain-filling patterns (Figures 1 and 6). This provides a possible explanation for the experimentally determined regime diagrams (for example, Figure 2 in [31] and Figure 2 in [25]).

In section 4.3 we presented a novel bifurcation diagram for (2.1)–(2.2) as it moves closer to our novel distinguished asymptotic limit. For the parameter values we used we observed that all except one of the saddle-nodes on the snaking branch had disappeared through a cusp bifurcation, leaving a monotonic curve of oscillons with no hysteresis between oscillons containing different numbers of pattern wavelengths. This rather extreme version of slanted snaking we called "smooth snaking." It was not observed in the related model problems discussed by Dawes [14] or Firth, Columbo, and Scroggie [18].

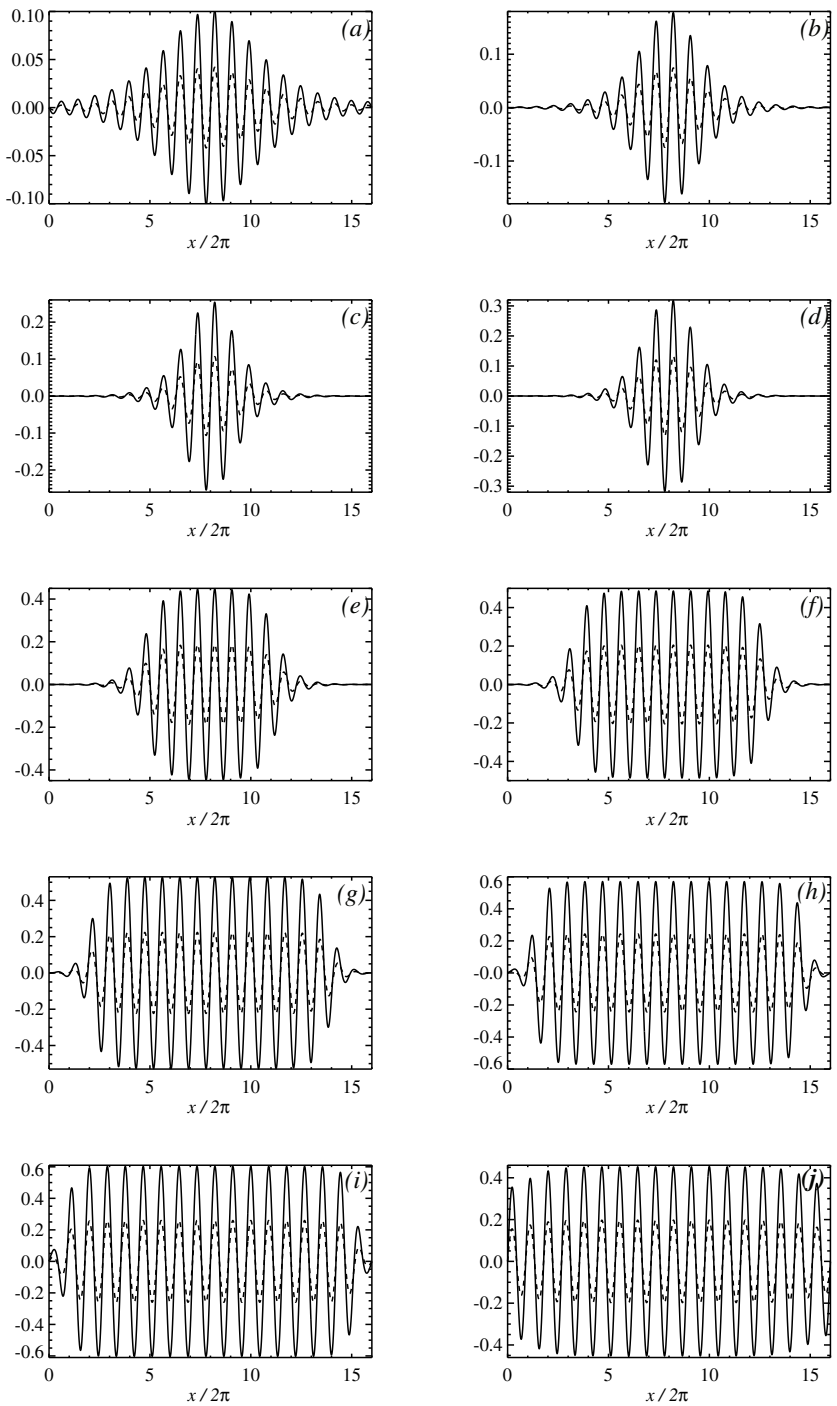

Figure 9. *Odd-symmetric steady-state solution profiles at the labels* a–j *indicated in Figure* 8. (a) $\gamma = 3.7074$; (b) $\gamma = 3.6946$; (c) $\gamma = 3.6809$; (d) $\gamma = 3.6732$; (e) $\gamma = 3.6858$; (f) $\gamma = 3.7071$; (g) $\gamma = 3.7329$; (h) $\gamma = 3.7619$; (i) $\gamma = 3.7869$; (j) $\gamma = 3.7192$. *Other parameters are as in Figure* 8.

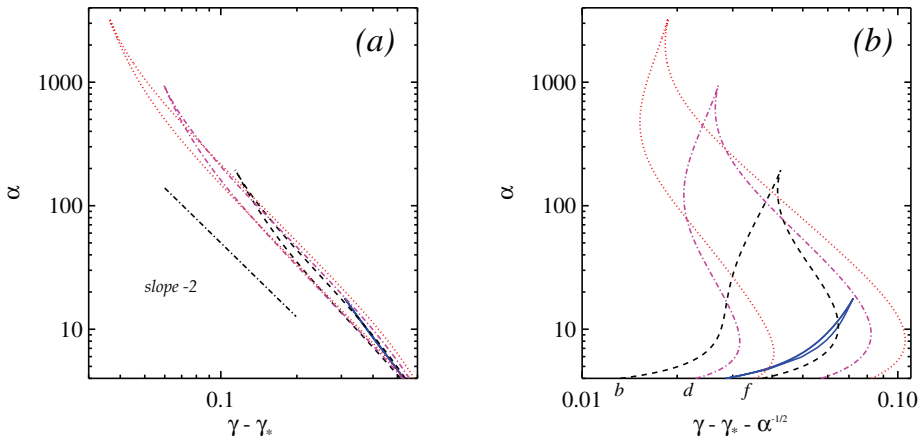

Figure 10. (a) *Cusp bifurcations in the* (γ, α) *plane as saddle-node bifurcations on the (odd-symmetric) snaking branch disappear as* α *increases.* (b) *is a replotting of the data in* (a). *Points* b, d, *and* f *on the line* $\alpha = 4$ *in* (b) *correspond to the labels in Figure* 1(b) *and the corresponding parts of Figure* 2. *Continuation is carried out in* α, *keeping all other parameters constant:* $\omega = h = 4$, $b = \beta = 1$, *domain size* $L = 32\pi$.

We have confirmed that the simple oscillon states, for example those on the parts of the snaking curves with positive gradients in Figure 1, very similar in profile to those shown in Figure 2, are stable in time by solving (2.1)–(2.2) using a timestepping code. We do not expect that the other localized states found are necessarily stable, and even if this were the case, their physical relevance would be highly dubious. In addition, we point out that the system (2.1)–(2.2) is not variational, and as a result it is possible that oscillons undergo additional oscillatory instabilities leading to quasi-periodic localized states. We have not investigated this possibility.

Two obvious lines of further enquiry present themselves: first, to treat axisymmetric solutions in two dimensions, which should correspond much better, perhaps even quantitatively, with experimental observations; second, to return to models derived on more physical grounds such as that proposed by Eggers and Riecke [17] and probe the bifurcation structure of the oscillon states found numerically in that work.

Acknowledgment. We are grateful to the referees for useful comments which have led to improvements in the presentation of this work.

REFERENCES

[1] I. S. Aranson and L. S. Tsimring, *Patterns and collective behaviour in granular media: Theoretical concepts*, Rev. Mod. Phys., 78 (2006), pp. 641–692.

[2] M. Beck, J. Knobloch, D. J. B. Lloyd, B. Sandstede, and T. Wagenknecht, *Snakes, ladders, and isolas of localized patterns*, SIAM J. Math. Anal., 41 (2009), pp. 936–972.

[3] D. Bensimon, B. I. Shraiman, and V. Croquette, *Nonadiabatic effects in convection*, Phys. Rev. A, 38 (1988), pp. 5461–5463.

[4] A. Bergeon, J. Burke, E. Knobloch, and I. Mercader, *Eckhaus instability and homoclinic snaking*, Phys. Rev. E, 78 (2008), paper 046201.

[5] J. Burke, A. Yochelis, and E. Knobloch, *Classification of spatially localized oscillations in periodically forced dissipative systems*, SIAM J. Appl. Dyn. Syst., 7 (2008), pp. 651–711.
[6] J. Burke and E. Knobloch, *Localized states in the generalized Swift–Hohenberg equation*, Phys. Rev. E, 73 (2006), paper 056211.
[7] J. Burke and E. Knobloch, *Snakes and ladders: Localized states in the Swift–Hohenberg equation*, Phys. Lett. A, 360 (2007), pp. 681–688.
[8] S. J. Chapman and G. Kozyreff, *Exponential asymptotics of localized patterns and snaking bifurcation diagrams*, Phys. D, 238 (2009), pp. 319–354.
[9] P. Coullet, T. Frisch, and G. Sonnino, *Dispersion-induced patterns*, Phys. Rev. E, 49 (1994), pp. 2087–2090.
[10] P. Coullet, C. Riera, and C. Tresser, *Stable static localized structures in one dimension*, Phys. Rev. Lett., 84 (2000), pp. 3069–3072.
[11] C. Crawford and H. Riecke, *Oscillon-type structures and their interaction in a Swift–Hohenberg model*, Phys. D, 129 (1999), pp. 83–92.
[12] M. C. Cross and P. C. Hohenberg, *Pattern formation outside of equilibrium*, Rev. Mod. Phys., 65 (1993), pp. 851–1112.
[13] J. H. P. Dawes, *Localized states in thermal convection with an imposed vertical magnetic field*, J. Fluid Mech., 570 (2007), pp. 385–406.
[14] J. H. P. Dawes, *Localized pattern formation with a large-scale mode: Slanted snaking*, SIAM J. Appl. Dyn. Syst., 7 (2008), pp. 186–206.
[15] J. H. P. Dawes, *Modulated and localized states in a finite domain*, SIAM J. Appl. Dyn. Syst., 8 (2009), pp. 909–930.
[16] E. J. Doedel, A. R Champneys, T. Fairgrieve, Y. Kuznetsov, B. Oldeman, R. Paffenroth, B. Sandstede, X. Wang, and C. Zhang, *AUTO-07p: Continuation and Bifurcation Software for Ordinary Differential Equations*, 2007; software available to download from http://indy.cs.concordia.ca/auto/.
[17] J. Eggers and H. Riecke, *Continuum description of vibrated sand*, Phys. Rev. E, 59 (1999), pp. 4476–4483.
[18] W. Firth, L. Columbo, and A. J. Scroggie, *Proposed resolution of theory-experiment discrepancy in homoclinic snaking*, Phys. Rev. Lett., 99 (2007), paper 104503.
[19] I. S. Gradshteyn and I. M. Ryzhik, *Table of Integrals, Series and Products*, 6th ed., A. Jeffrey and D. Zwillinger, eds., Academic Press, New York, 2000; http://www.mathtable.com/gr/.
[20] Y. Hiraoka and T. Ogawa, *Rigorous numerics for localized patterns to the quintic Swift–Hohenberg equation*, Japan J. Ind. Appl. Math., 22 (2005), pp. 57–75.
[21] R. B. Hoyle, *Pattern Formation: An Introduction to Methods*, Cambridge University Press, Cambridge, UK, 2006.
[22] G. Iooss and M.-C. Perouème, *Periodic homoclinic solutions in reversible* 1:1 *resonance vector fields*, J. Differential Equations, 102 (1993), pp. 62–88.
[23] G. Kozyreff and S. J. Chapman, *Asymptotics of large bound states of localized structures*, Phys. Rev. Lett., 97 (2006), paper 044502.
[24] O. Lioubashevski, H. Arbell, and J. Fineberg, *Dissipative solitary states in driven surface waves*, Phys. Rev. Lett., 76 (1996), pp. 3959–3962.
[25] O. Lioubashevski, Y. Hamiel, A. Agnon, Z. Reches, and J. Fineberg, *Oscillons and propagating solitary waves in a vertically vibrated colloidal suspension*, Phys. Rev. Lett., 83 (1999), pp. 3190–3193.
[26] P. C. Matthews and S. M. Cox, *Pattern formation with a conservation law*, Nonlinearity, 13 (2000), pp. 1293–1320.
[27] L. M. Pismen, *Patterns and Interfaces in Dissipative Dynamics*, Springer, Berlin, 2006.
[28] Y. Pomeau, *Front motion, metastability and subcritical bifurcations in hydrodynamics*, Phys. D, 23 (1986), pp. 3–11.
[29] H. Sakaguchi and H. R. Brand, *Stable localized solutions of arbitrary length for the quintic Swift–Hohenberg equation*, Phys. D, 97 (1996), pp. 274–285.
[30] L. S. Tsimring and I. S. Aranson, *Localized and cellular patterns in a vibrated granular layer*, Phys. Rev. Lett., 79 (1997), pp. 213–216.

[31] P. Umbanhowar, F. Melo, and H. L. Swinney, *Localized excitations in a vertically vibrated granular layer*, Nature, 382 (1996), pp. 793–796.
[32] D. M. Winterbottom, S. M. Cox, and P. C. Matthews, *Pattern formation in a model of a vibrated granular layer*, SIAM J. Appl. Dyn. Syst., 7 (2008), pp. 63–78.
[33] P. D. Woods and A. R. Champneys, *Heteroclinic tangles and homoclinic snaking in the unfolding of a degenerate reversible Hamiltonian–Hopf bifurcation*, Phys. D, 129 (1999), pp. 147–170.